3-Dimensional Imaging and Motion Estimation Method of Multiple Moving Targets for Multi-Static UWB Radar Using Target Point and Its Normal Vector

Ryo YAMAGUCHI[†], Shouhei KIDERA[††a)], *and* Tetsuo KIRIMOTO[††], *Members*

SUMMARY   Radar systems using ultra-wideband (UWB) signals have definitive advantages in high range resolution. These are suitable for accurate 3-dimensional (3-D) sensing by rescue robots operating in disaster zone settings, where optical sensing is not applicable because of thick smog or high-density gas. For such applications, where no *a priori* information of target shape and position is given, an accurate method for 3-D imaging and motion estimation is strongly required for effective target recognition. In addressing this issue, we have already proposed a nonparametric 2-dimensional (2-D) imaging method for a target with arbitrary target shape and motion including rotation and translation being tracked using a multi-static radar system. This is based on matching target boundary points obtained using the range points migration (RPM) method extended to the multi-static radar system. Whereas this method accomplishes accurate imaging and motion estimation for single targets, accuracy is degraded severely for multiple targets, due to interference effects. For a solution of this difficulty, this paper proposes a method based on a novel matching scheme using not only target points but also normal vectors on the target boundary estimated by the Envelope method; interference effects are effectively suppressed when incorporating the RPM approach. Results from numerical simulations for both 2-D and 3-D models show that the proposed method simultaneously achieves accurate target imaging and motion tracking, even for multiple moving targets.

key words: *UWB radar, multiple moving targets, range points migration (RPM), interference suppression, multi-static UWB radar*

1.   Introduction

Ultra-wideband (UWB) pulse radar with high range resolution is one of the most promising techniques for comparatively near-field image sensing for rescue robots, because it is applicable to situations where optical sensing is ineffective such as environments where heavy smoke, nebulous gas or strong backlighting prevail. While various kinds of radar imaging methods have been proposed [1]–[5], there are substantial problems in image accuracy, spatial resolution or computational cost. The range points migration (RPM) method has established itself as one of the more efficient 3-D imaging methods [6]; this method is based on the group mapping of observed range points to target boundary points through accurate direction-of-arrival (DOA) estima-

tion, and retains a sufficient accuracy even for complicated target boundaries or in noisy surroundings. However, the original RPM method assumes single static targets, despite the imaging of moving targets such as people being indispensable in disaster scenes or other scenarios.

There has been much research on the detection and localization of moving targets with radar systems with the focus mainly on far-field measurements and specifying targets as consisting of an aggregate of multiple point targets [7], [8]. However, the imaging accuracy of these methods should basically degrade with near-field measurements, because the scattering center moves continually on the target surface producing large dynamic changes in the observation angle and the assumption for multiple point targets is no longer valid. To substantially address such issues, a method [9] was proposed in which, using distances measured from a small number of antennas, the local shape of the target is approximated in model fitting by a segment of an ellipse. Whereas this method works well for several types of target shapes that are similar to ellipses, unavoidably, image accuracy is compromised for non-elliptical shapes, as demonstrated in [10].

In surmounting this problem, we have already proposed an imaging and motion estimation method for targets with arbitrary shape [10]. Here the RPM method is introduced to provide non-parametric imaging, where it is extended to multi-static targets so that a sufficient number of target boundary points for motion estimation are obtained in less data acquisition time. The motion estimation of this method is based on a matching scheme using RPM for target points for consecutive observation times; this method simultaneously determines target shape and motion without assuming any target shape model.

However, the method [10] has a significant problem in that, for multiple targets, the motion estimation accuracy, especially for rotation angles, is severely degraded from interference effects between the targets. Thus, this paper provides a substantial revision of the previous method [10], particularly by incorporating the RPM and the Envelope method [11] to suppress the interference and a matching scheme for motion estimation using not only a target point but also its normal vector. In particular, using the unique feature of the RPM method, i.e., correct target clustering, each observed range point corresponding to each clustered target is also clearly discriminated; this helps in finding the

interference region. Next, the Envelope method is introduced for estimating not only target points but also normal vectors on each clustered target boundary that mainly contributes to improving the accuracy in estimates of rotation of the moving target. It is a notable feature of the RPM or Envelope method that each normal vector on the target boundary can be calculated without using the spatial difference approach. In addition, the proposed method can be extended naturally to the 3-D observation model in practical applications. The results obtained from numerical simulations, including both the 2-D and 3-D models in noisy environments, verify the effectiveness of the proposed method from both quantitative and statistical points of view.

This paper is organized as follows. In Sect. 2, for simplicity of description, the system model assuming multistatic observation in the 2-D model is presented. Section 3 briefly explains the conventional method [10] and clarifies those problems mentioned above. Section 4 describes in detail the principle and methodology of the proposed method including the target clustering approach with RPM method for interference suppression and the normal vector matching schemes by employing the Envelope method. Section 5 presents results from numerical simulations of imaging and motion estimation for each method in the 2-D model; quantitative analysis is also provided. The 3-D model extension of the proposed methodology and a performance evaluation is described in Sect. 6. Finally, concluding remarks are given in Sect. 7.

2. System Model

The system model is shown in Fig. 1. For simplicity of description, Sects. 2–5 cover the 2-D problem of target tracking using just the transverse electric modes. The target is assumed to have an arbitrary fixed shape with a clear boundary moving arbitrarily, i.e., rotating and translating. A number (greater than two) of omni-directional antennas are arranged along the x-axis at fixed intervals to form a multi-static radar configuration. The transmitting signal is a mono-cycle
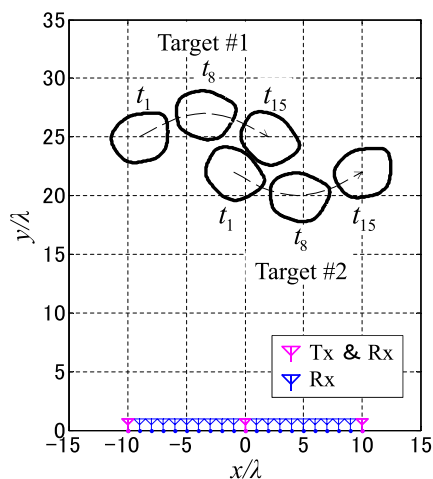

Fig. 1 System model in two-dimensional problems.

pulse; its central wavelength is denoted by λ and its fractional bandwidth defined in [12] is about 100%. The actual wavelength used in practical situations has been discussed in [10]. Here, the observational data are assumed to be acquired almost instantaneously so that the target motion during the data acquisition interval is negligible. The n-th observation time is defined as $t_n = (n-1)\Delta t$ $(1 \le n \le N)$, where Δt denotes the interval between consecutive observation event. The locations of the transmitting and receiving antennas are defined as $\boldsymbol{L}_T = (X_T, 0)$ and $\boldsymbol{L}_R = (X_R, 0)$, respectively. For each combination of $\boldsymbol{L}_T$ and $\boldsymbol{L}_R$, the output of the Wiener filter is denoted $s(\boldsymbol{q}')$, where $\boldsymbol{q}' = (\boldsymbol{L}_T, \boldsymbol{L}_R, r')^T$ is defined with $r' = c\tau/2$, delay time τ and speed of the radio wave c. $\boldsymbol{q} = (\boldsymbol{L}_T, \boldsymbol{L}_R, r)^T$ is the range point, which is extracted from the local maxima of $s(\boldsymbol{q}')$ as to r', where r denotes the extracted range. This procedure is summarized in [6].

3. Conventional Method

As one of the most effective conventional imaging methods for moving targets, this section briefly describes our previous work [10], which is based on the matching scheme. First, this method obtains the target boundary points using the multi-static RPM method to the range points; this basically can be applied to a multiple number of objects. To treat multiple targets, the target boundary points at the n-th observation time are clustered according to Euclidean distances; the same approach is detailed in [13]. The target boundary points classified into the k-th cluster at the n-th observation time are defined as $\boldsymbol{p}_{i,k}^{(n)}$, $\boldsymbol{e}_{i,k}^{(n)}$ $\left(i = 1, \cdots, M_k^{(n)}\right)$, where $M_k^{(n)}$ denotes the number of the target boundary points classified into the k-th cluster. The target boundary point after rotation and translation of $\boldsymbol{p}_{j,k}^{(n-1)}$ is expressed as

$$\tilde{\boldsymbol{p}}_{j,k}^{(n)} = \boldsymbol{R}\left\{\boldsymbol{p}_{j,k}^{(n-1)} - \boldsymbol{C}_k^{(n-1)}\right\} + \boldsymbol{C}_k^{(n-1)} + \boldsymbol{T}, \tag{1}$$

where $\boldsymbol{R}$ denotes the rotation matrix, $\boldsymbol{T}$ denotes the translation motion vector and $\boldsymbol{C}_k^{(n-1)}$ denotes the barycentric position of the target boundary points calculated from a set $\boldsymbol{p}_{j,k}^{(n-1)}$. For motion estimation, the cost function is defined as

$$F_k^{(n)} = \frac{1}{M_k^{(n-1)}} \sum_{j=1}^{M_k^{(n-1)}} \min_i \left\| \boldsymbol{p}_{i,k}^{(n)} - \tilde{\boldsymbol{p}}_{j,k}^{(n)} \right\|^2. \tag{2}$$

Figure 2 shows the spatial relationship between $\boldsymbol{p}_{i,k}^{(n)}$ and $\tilde{\boldsymbol{p}}_{j,k}^{(n)}$. This method determines the target motion $\boldsymbol{R}_k^{(n)}$ and $\boldsymbol{T}_k^{(n)}$ over time interval t_{n-1} to t_n as

$$\left(\boldsymbol{R}_k^{(n)}, \boldsymbol{T}_k^{(n)}\right) = \arg\min_{(\boldsymbol{R}, \boldsymbol{T})} F_k^{(n)}. \tag{3}$$

Whereas this method retains sufficient accuracy for shape and motion estimation for a single target, for multiple targets, accuracy is severely degraded mainly due to interference effects from the various targets. In particular, for the rotation angle, estimates of accuracy are difficult to obtain.
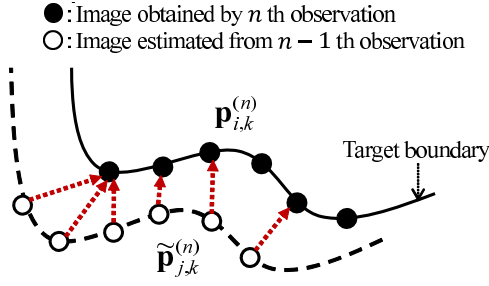
Fig. 2 Relationship between $p_{i,k}^{(n)}$ and $\tilde{p}_{j,k}^{(n)}$ of the conventional method in Eq. (2).

Fig. 3 Interference suppression of $q_{i,k}$. ($n = 14$, $X_T = -10\lambda$)

Fig. 4 Relationship between $p_{i,k}^{(n)}$, $e_{i,k}^{(n)}$, $\tilde{p}_{j,k}^{(n)}$ and $\tilde{e}_{j,k}^{(n)}$ of the proposed method in Eq. (4).

4. Proposed Method

As a solution for the problem mentioned in the previous section, the two significant revisions of the above conventional method are newly introduced in this paper, which incorporates an interference suppression scheme by exploiting an one-to-one correspondence between a target and range point and adopting a novel matching approach employing the normal vector on target boundary obtained by the Envelope method.

First, the principle of the interference suppression scheme is briefly explained as follows. This scheme exploits a notable feature of the RPM method in that it obtains each target boundary point from the interference signal with sufficient accuracy to correctly cluster each target, which has been already demonstrated in [13]. Then, using the feature of the RPM that each range and target point satisfies the one-to-one correspondence, the range points, that are affected severely by interference, are removed from the total set of range points. Figure 3 shows an example of interference at $X_T = -10\lambda$, where the range points belonging to two clusters (marked in blue and red) are observed at almost the same range gate at $X_R = 3.0\lambda, 4.0\lambda$. In this antenna region, only a single range point is observed, the other is obscured by the interference effect. In contrast, using RPM imaging and clustering, we can recognize a correct cluster for each range point and can assess quantitatively its interference effect using range points belonging to other clusters. The detail formulation for the above scheme is described in the procedure of the proposed method, particular for Steps 2) and 3).

Second, the matching scheme of the target motion estimation is extended to use normal vectors on the target boundary as well as target points. These normal vectors mainly contribute to rotation estimations of the moving target. Here, to extract highly accurate unit normal vectors, the Envelope method [11] is applied to the range points after the clustering procedure of the target boundary points obtained by the multi-static RPM. While in principle the Envelope method is applicable to arbitrarily shaped targets [11], in the case of multiple objects or complex-shaped objects, this method requires a correct separation of the range points belonging to each target or part of a target, because it only as-
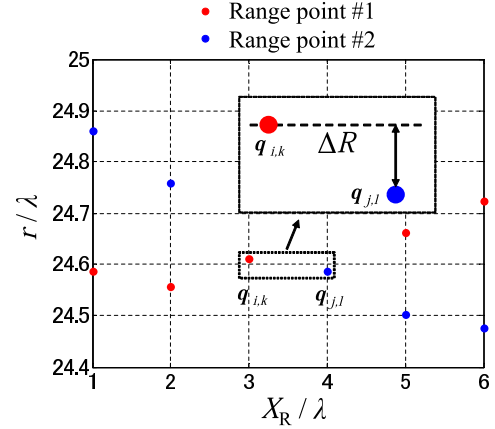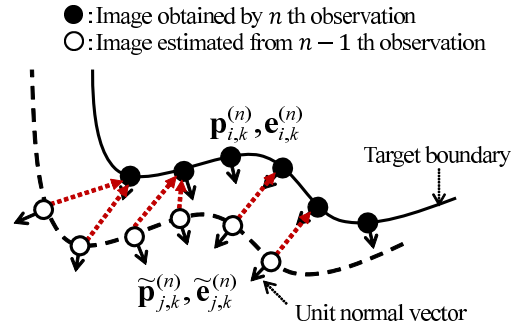
sesses the outer or inner boundary of the circles determined by a grouped range points. In contrast, the Envelope method can estimate the target points and normal vectors more accurately than the RPM method, thereby enhancing the accuracy of motion estimations. This is the reason why we employ the RPM method for target clustering and the Envelope method for calculating a target boundary and its normal vector. Here, the mono-static type of Envelope method is readily extended to the multi-static type, where the target boundary is expressed as the envelope of ellipse focal points on the locations of the transmitting and the receiving antennas. A novel cost function has been accordingly developed

$$G_k^{(n)} = \frac{1}{M_k^{(n-1)}} \sum_{j=1}^{M_k^{(n-1)}} \min_i \left[\left\| p_{i,k}^{(n)} - \tilde{p}_{j,k}^{(n)} \right\|^2 + \alpha \left\| e_{i,k}^{(n)} - \tilde{e}_{j,k}^{(n)} \right\|^2 \right]. \quad (4)$$

Here, $p_{i,k}^{(n)}$ and $e_{i,k}^{(n)}$ denote the target boundary points and the unit normal vectors obtained by the Envelope method, $\tilde{e}_{j,k}^{(n)}$ is obtained from

$$\tilde{e}_{j,k}^{(n)} = R e_{j,k}^{(n-1)}, \quad (5)$$

and α denotes the regularization parameter, which is empirically determined. Figure 4 shows the spatial relationship between $p_{i,k}^{(n)}$, $e_{i,k}^{(n)}$, $\tilde{p}_{j,k}^{(n)}$ and $\tilde{e}_{j,k}^{(n)}$. This method determines the target motion $R_k^{(n)}$ and $T_k^{(n)}$ from t_{n-1} to t_n as
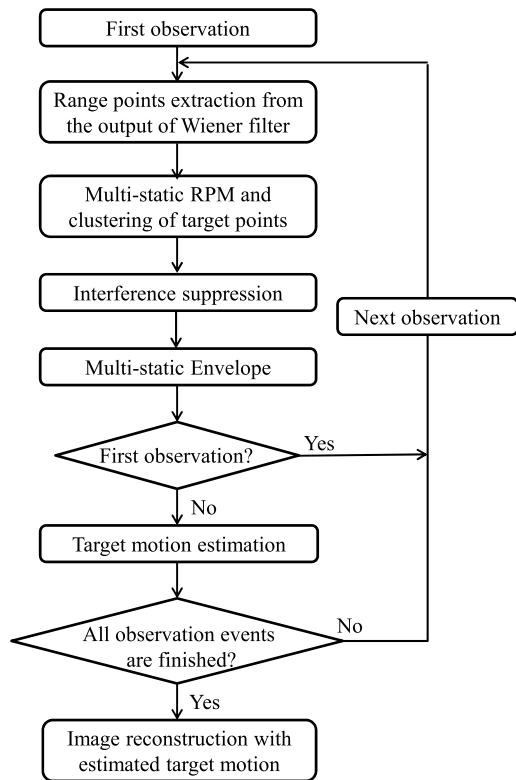
First observation

Range points extraction from
the output of Wiener filter

Multi-static RPM and
clustering of target points

Interference suppression

Next observation

Multi-static Envelope

First observation? — Yes

No

Target motion estimation

All observation events
are finished? — No

Yes

Image reconstruction with
estimated target motion

Fig. 5   Flowchart of the proposed method.

$$\left(\boldsymbol{R}_k^{(n)}, \boldsymbol{T}_k^{(n)}\right) = \underset{(\boldsymbol{R},\boldsymbol{T})}{\arg\min}\, G_k^{(n)}. \tag{6}$$

The procedure for the proposed method (see Fig. 5 for a flowchart) is summarized as follows. First, $n = 1$ is set.

Step 1).   A set of target boundary points $\boldsymbol{p}_i^{(n)}\big(i = 1, \cdots, M_{\mathrm{p}}^{(n)}\big)$ is obtained by applying multi-static RPM to the observed range points $\boldsymbol{q}_i^{(n)}$.

Step 2).   Target boundary points are clustered based on the Euclidean distance.

Step 3).   Interference suppression method is applied to the range points in each cluster as follows. If $\Delta R\big(\boldsymbol{q}_{i,k}\big) < R_{\mathrm{th}}$ satisfied, $\boldsymbol{q}_{i,k}$ is removed. Here $\Delta R\big(\boldsymbol{q}_{i,k}\big) = |r_{i,k} - r_{j,l}|$. $r_{i,k}$ and $r_{j,l}$ denote each range of range points of $\boldsymbol{q}_{i,k}$ and $\boldsymbol{q}_{j,l}$, respectively, and the antenna position of $\boldsymbol{q}_{j,l}$ is adjacent to that of $\boldsymbol{q}_{i,k}$. Figure 3 also shows the relationship between $\boldsymbol{q}_{i,k}$ and $\boldsymbol{q}_{j,l}$. In addition, $i \neq j$ holds, which means that we should assess the accumulation degree of the range points excluding those of the same cluster (namely i th cluster). R_{th} is the threshold value, and is set around λ, where an interference between reflection echoes should be occurred.

Step 4).   Target boundary points and their unit normal vectors are interpolated by multi-static Envelope method in each cluster.

Step 5).   If $n \geq 2$ holds, go to Step 6); otherwise set $n = n + 1$ and return to Step 1).

Step 6).   The target motion $\boldsymbol{R}_k^{(n)}$ and $\boldsymbol{T}_k^{(n)}$ are estimated us-

ing $\boldsymbol{p}_{j,k}^{(n-1)}\big(j = 1, \cdots, M_{\mathrm{p}}^{(n-1)}\big)$ and $\boldsymbol{p}_{i,k}^{(n)}\big(i = 1, \cdots, M_{\mathrm{p}}^{(n)}\big)$.

Step 7).   If $n = N$ holds, go to Step 8); otherwise set $n = n + 1$ and return to Step 1).

Step 8).   A final target image is reconstructed with the estimated target motion in each cluster.

The proposed method has a significant advantage in that it can remove the inaccuracy range points severely affected by interference, and can enhance the accuracy in motion estimations, particularly for the rotation angle, by exploiting the normal vectors obtained by the Envelope method.

5.   Performance Evaluation in Numerical Simulations

This section investigates the performance of the conventional and proposed methods through numerical simulations in the 2-D model. The target shape is assumed as depicted in Fig. 1. The motion of the barycentric point $(x_{\mathrm{G}}^{(n)}, y_{\mathrm{G}}^{(n)})$ of the target at the n-th observation time is expressed as

$$\left.\begin{array}{l} x_{\mathrm{G}}^{(n)} = x_0 + v_x t_n \\ y_{\mathrm{G}}^{(n)} = y_0 + v_y \sin(\omega t_n) \end{array}\right\}, \quad (n = 1, \cdots, N), \tag{7}$$

and the rotation angle of the target is set as

$$\phi^{(n)} = \phi_0 \cos(\omega t_n), \quad (n = 1, \cdots, N), \tag{8}$$

where the parameters of target ♯1 is that $(x_0, y_0) = (-9.0\lambda, 25\lambda)$, $v_x = 0.79\lambda/\Delta t$, $v_y = 2.0\,\lambda/\Delta t$, $\omega = \pi/\{(N-1)\Delta t\}$, $N = 15$ and $\phi_0 = 0.52$ rad, and the parameters of target ♯2 is that $(x_0, y_0) = (-1.0\lambda, 22\lambda)$, $v_x = 0.79\lambda/\Delta t$, $v_y = -2.0\,\lambda/\Delta t$, $\omega = \pi/\{(N-1)\Delta t\}$, $N = 15$ and $\phi_0 = -0.52$ rad. It is assumed that the target maintains the same orientation relative to the direction of translational motion, such as when humans walk. Three transmitting antennas are located at $-10.0\lambda \leq x \leq 10.0\lambda$ at intervals of 10.0λ, and 21 receiving antennas are located at $-10.0\lambda \leq x \leq 10.0\lambda$ at intervals of λ. This is because in multi-receiving systems, the total acquisition time depends mainly on the switching time for the transmitting antennas. Here, the received data are analyzed using the geometric optics approximation, which is also used in [13], so as to assess the far-field observation. While this type of data generation does not consider multiple scattering effects and frequency dependency of scattering phenomena, as reported in [14], we assume in this case only a single target of size sufficiently larger than the wavelength or one having no edge, for then the frequency dependency of scattering is negligible.

Figures 6 and 7 show the target boundary points obtained using the conventional and proposed imaging approaches at three observation times at S/N = 25 dB. Here, Gaussian white noise is added to the received signals, and the signal-to-noise ratio S/N is defined as the ratio of the peak instantaneous signal power to average noise power after applying a matched filter. Figures 8(a) and (b) depicts the unit normal vectors of each target boundary point obtained using the conventional and proposed imaging approaches, respectively. These figures indicate that the proposed method can enhance not only the accuracy in target
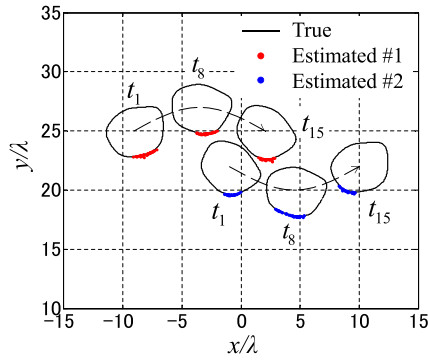
Fig. 6 Target boundary points obtained by the conventional imaging approach after clustering operation in S/N = 25 dB at t_1, t_8 and t_{15}.
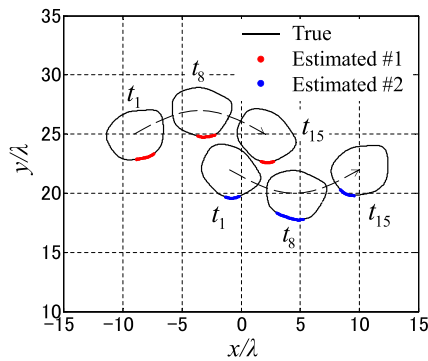

Fig. 7 Target boundary points obtained by the proposed imaging approach in S/N = 25 dB at t_1, t_8 and t_{15}.
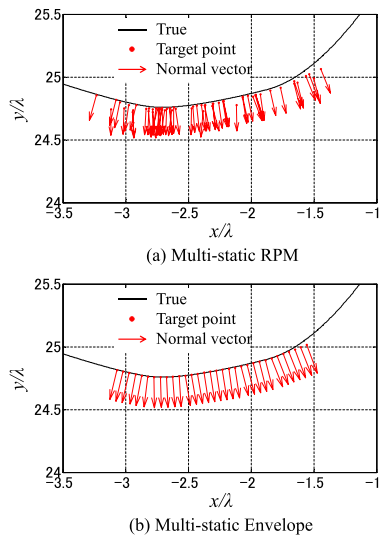

(a) Multi-static RPM

(b) Multi-static Envelope

Fig. 8 Comparison of the unit normal vectors obtained multi-static RPM method and Envelope method ((a) Multi-static RPM (b) Multi-static Envelope).

(a) Rotational angle

(b) Translation for x-axis

(c) Translation for y-axis

Fig. 9 Motion of target ♯1 for each observation time estimated by the conventional and proposed method in S/N = 25 dB. ((a) Difference value of rotation angle (b) Difference value of translation motion for x-axis (c) Difference value of translation motion for y-axis.)

(a) Rotational angle

(b) Translation for x-axis

(c) Translation for y-axis

Fig. 10 Motion of target ♯2 for each observation time estimated by the conventional and proposed method in S/N = 25 dB. ((a) Difference value of rotation angle (b) Difference value of translation motion for x-axis (c) Difference value of translation motion for y-axis.)

points but also the corresponding normal vectors. This beneficial result is mainly contributed by an elaborate combination of the RPM (correct clustering) and Envelope (accurate normal vector estimation) features. Using again both methods, Figs. 9 and 10 show the estimated motion of tar-
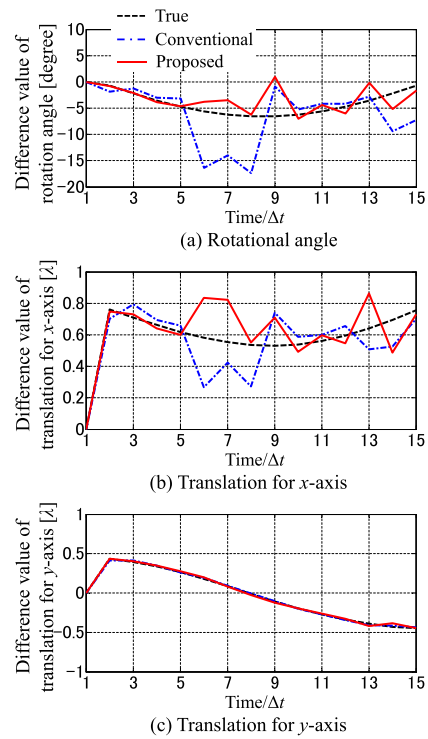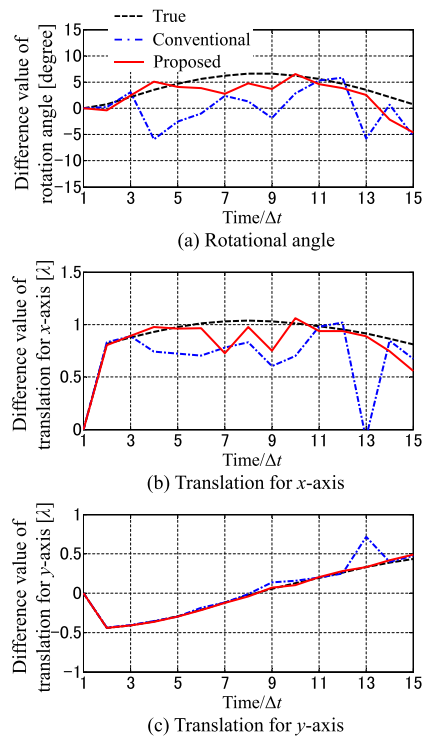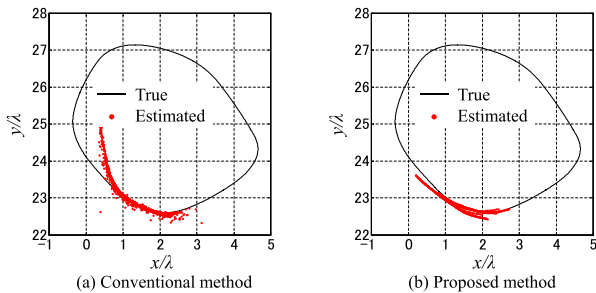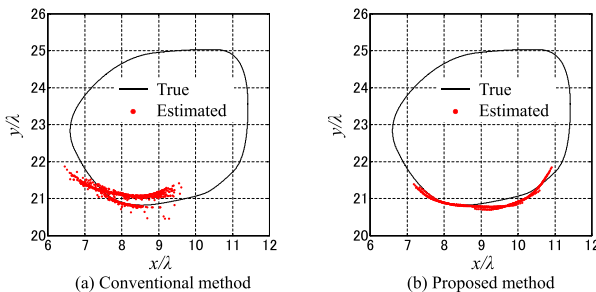
Fig. 11 Reconstructed image of target ♯1 in S/N = 25 dB. ((a) Conventional method (b) Proposed method.)


Fig. 12 Reconstructed image of target ♯2 in S/N = 25 dB. ((a) Conventional method (b) Proposed method.)

gets ♯1 and ♯2 where the vertical axes of (a)–(c) denote the difference between consecutive observation times of the rotation angle, the translation value for x-axis, and that for y-axis, respectively. Here, the parameters for the proposed method are set as $\alpha = 1.0$ and $R_{\mathrm{th}} = 1.0\lambda$, and the interpolation interval of Envelope method is set to 0.05λ. The Particle Swarm Optimization algorithm [15], [16] is employed to obtain a global optimum of Eq. (3) in the conventional method or Eq. (6) in the proposed method. The results obtained using the conventional method show that the motion estimation accuracy diminishes for each target because positioning inaccuracies accrue for the target boundary points using the multi-static RPM. In contrast, the results obtained from the proposed method demonstrate that each estimated motion is accurately tracked even for multiple targets, thus this method has a notable advantage over the conventional method. As a final image comparison, Figs. 11 and 12 show the target shape for targets ♯1 and ♯2 compensated by the target motion estimated with the conventional and proposed methods. These results also verify that the proposed method successfully expands the image area of the target boundary with higher accuracy compared to that obtained using the conventional method.

For quantitative analysis from a statistical viewpoint, $\epsilon(x_{\mathrm{e}}^{i})$ is introduced as

$$\epsilon\left(x_{\mathrm{e}}^{i}\right) = \min_{x}\left\|x - x_{\mathrm{e}}^{i}\right\|, \ (i = 1, 2, \cdots, N_{\mathrm{T}}), \qquad (9)$$

where x and x_{e}^{i} denote respectively the locations of the true target points and the estimated target points of the final image reconstructed with the proposed method. N_{T} is the total
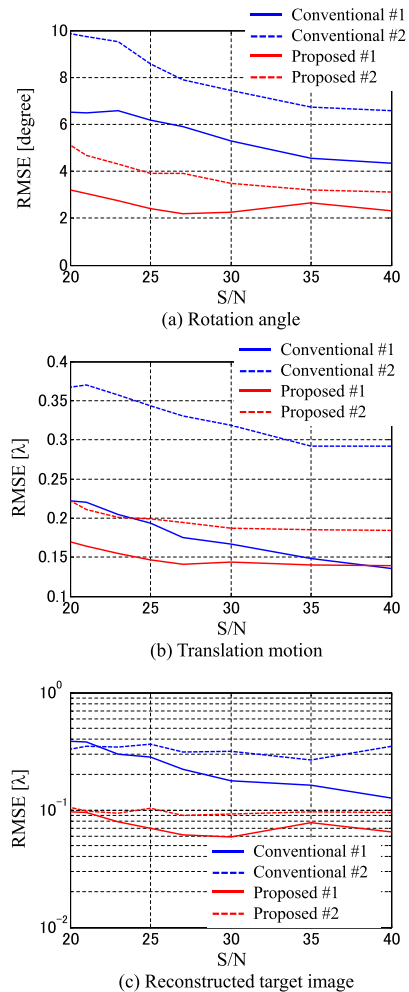
Fig. 13 Each RMSE versus S/N for the proposed method. ((a) Rotation angle (b) Translation motion (c) Reconstructed target image.)

number of x_{e}^{i}. Figure 13 illustrates the relationship between the RMSE (Root Mean Square Error) for the estimated rotation angles (a), translation motion (b) and the reconstructed image (c), whose error is defined as $\epsilon(x_{e}^{i})$, versus S/N for each method. Here, at each S/N value, the number of Monte-Carlo trials is set to 100, and each RMS error is the average for this number of trials. These results indicate that the proposed method performs better than the conventional method at all S/N values.

Furthermore, we mention a performance limitation of the proposed method assuming this observation model. From the qualitative viewpoint derived from the principle of the proposed method, it can be expected that when the distance between multiple objects becomes shorter, the motion and shape estimation of the proposed method (also the conventional method) becomes more difficult because of incorrect clustering, or insufficient suppression of interference effect. It also should be noted that this method requires a significant assumption in that any one target is not shadowed by others because a sequential temporal tracking of the target image is needed. In addition, the performance of

the proposed method basically depends on the presumed parameters, especially the threshold for clustering as R_{th} or the temporal sampling rate over observation time as Δt. More investigations and improvements in methods to overcome these challenging issues forms part of the aims of future work.

6. Extension to Three-Dimensional Problem

6.1 System and Methodology Extension

This section describes the extensions of both the conventional and proposed method to handle 3-D target system models illustrated in Fig. 14. The target model, antenna, and transmitting signal are the same as those assumed in the 2-D problem. Target rotations and translations each have now three degrees of freedom. A number (greater than three) of omni-directional antennas are arranged in an array on the $y = 0$ plane to form a multi-static radar configuration. The transmitted wave is assumed polarized along the z-axis direction. The locations of the transmitting and receiving antennas are defined as $\boldsymbol{L}_T = (X_T, 0, Z_T)$ and $\boldsymbol{L}_R = (X_R, 0, Z_R)$, respectively. $\boldsymbol{q} = (\boldsymbol{L}_T, \boldsymbol{L}_R, r)^T$ is the range point defined as in 2-D problem.

Both conventional and proposed methods are easily extended to handle a 3-D model; each parameter in Eqs. (1)–(6) is modified to accommodate $\boldsymbol{R}$ and $\boldsymbol{T}$ having three degrees of freedom. The estimated target boundary points $\boldsymbol{p}_{i,k}^{(n)}$ and their unit normal vectors $\boldsymbol{e}_{i,k}^{(n)}$ now depend on the parameters x, y, and z.

6.2 Performance Evaluation in Numerical Simulations

This section describes the performance evaluations for the conventional and proposed methods on the given 3-D system model assuming the target shape of Fig. 14. Nine transmitting antennas, arranged on the $y = 0$ plane, are located at $-10.0\lambda \le x \le 10.0\lambda$ and $5.0\lambda \le z \le 15.0\lambda$, and 45 receiving antennas are located at $-10.0\lambda \le x \le 10.0\lambda$ at intervals of 2.5λ in a reticular pattern. The motion of barycentric point $(x_G^{(n)}, y_G^{(n)}, z_G^{(n)})$ of the target at the n-th observation time is set as

$$\left.\begin{aligned} x_G^{(n)} &= x_0 + v_x t_n \\ y_G^{(n)} &= y_0 + v_y \sin(\omega t_n) \\ z_G^{(n)} &= z_0 \end{aligned}\right\}, \quad (n = 1, \cdots, N), \tag{10}$$

and the angle of target rotation is set as

$$\phi^{(n)} = \phi_0 \cos(\omega t_n), \quad (n = 1, \cdots, N), \tag{11}$$

where the parameters of target $\sharp 1$ are that $(x_0, y_0, z_0) = (-9.0\lambda, 25\lambda, 10\lambda)$, $v_x = 0.79\lambda/\Delta t$, $v_y = 2.0 \ \lambda/\Delta t$, $\omega = \pi/\{(N-1)\Delta t\}$, $N = 15$ and $\phi_0 = 0.52$ rad, and those of target $\sharp 2$ are that $(x_0, y_0, z_0) = (-1.0\lambda, 22\lambda, 10\lambda)$, $v_x = 0.79\lambda/\Delta t$, $v_y = -2.0 \ \lambda/\Delta t$, $\omega = \pi/\{(N-1)\Delta t\}$, $N = 15$ and $\phi_0 = -0.52$ rad, respectively.

Figures 15 and 16 show the target boundary points obtained by the multi-static RPM and the Envelope method at each observation time at S/N = 25 dB. Figures 17 and 18 show the estimated motion of targets $\sharp 1$ and $\sharp 2$ obtained by the conventional and proposed methods, where the vertical axes of (a)–(f) denote differences between consecutive observation times for each of the three rotation angles and three translation components along the x-axis, y-axis, and z-axis. Here, the parameters α and R_{th} for the proposed method are used the same values assumed in the 2-dimensional model. To reduce computational burden, the interpolation interval of 3-dimensional Envelope method is set to 0.1λ. Whereas Figs. 15 and 16 apparently show that both the conventional and proposed methods can accurately estimate each target boundary points, Figs. 17 and 18 demonstrate that the motion estimation accuracy of the conventional method is severely degraded compared with that obtained from the proposed method, because each normal vector on the target boundary can be accurately estimated even given 3-D models. This contributes to accuracy improvements, especially for the rotation angles. As a final image comparison, Figs. 19 and 20 show the target shapes compensated for target motion estimated with the conventional and proposed methods for targets $\sharp 1$ and $\sharp 2$. These results also demonstrate that, owing to the more accurate motion estimations, the proposed method has been successful in accurately expanding the image area of the target boundary
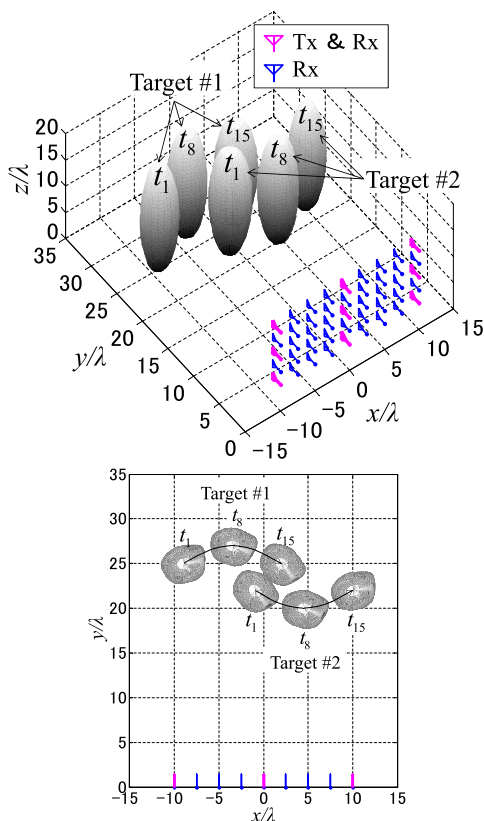

Fig. 14 System model in 3-D problems. (Upper:3-dimensional view. Lower:projected image on the $x - y$ plane.)
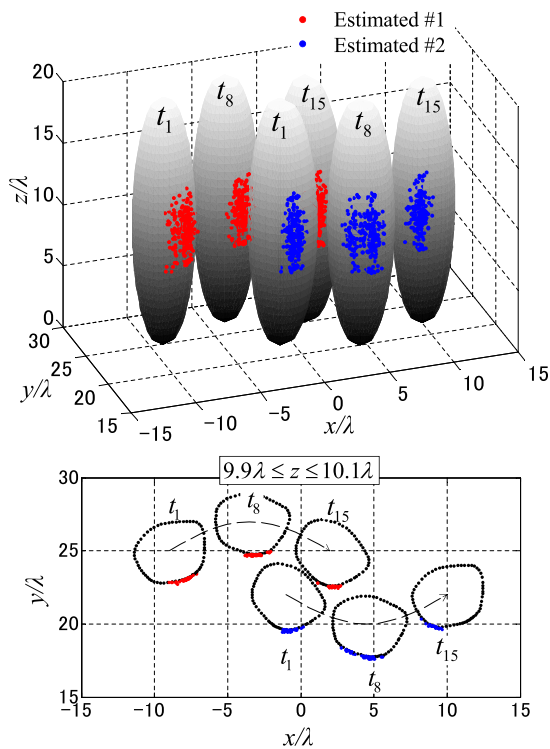
Fig. 15 Target boundary points obtained by the multi-static RPM method after clustering operation in S/N = 25 dB at t_1, t_8 and t_{15}. (Upper:3-dimensional view. Lower: cross section image for $9.9 \leq z \leq 10.1\lambda$.)
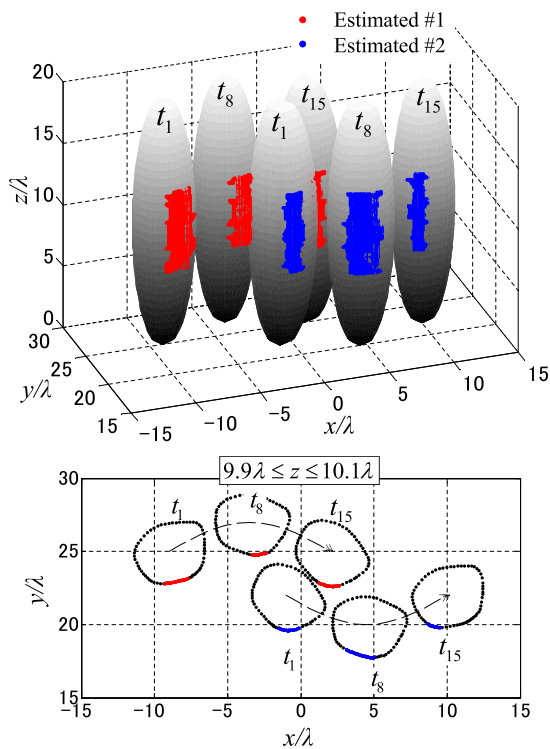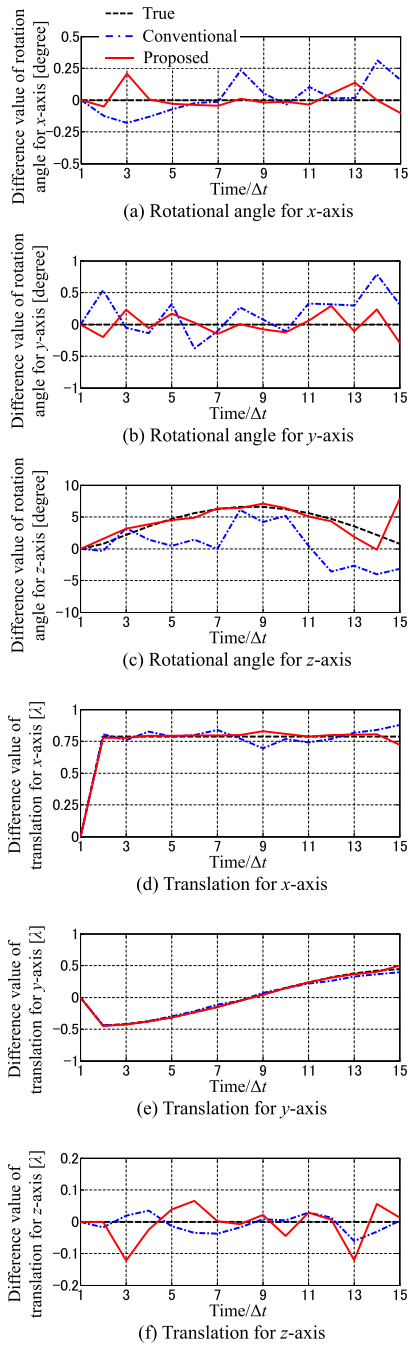

Fig. 16 Target boundary points obtained by the proposed method in S/N = 25 dB at t_1, t_8 and t_{15}. (upper: 3-dimensional view, lower: cross section image for $9.9 \leq z \leq 10.1\lambda$).
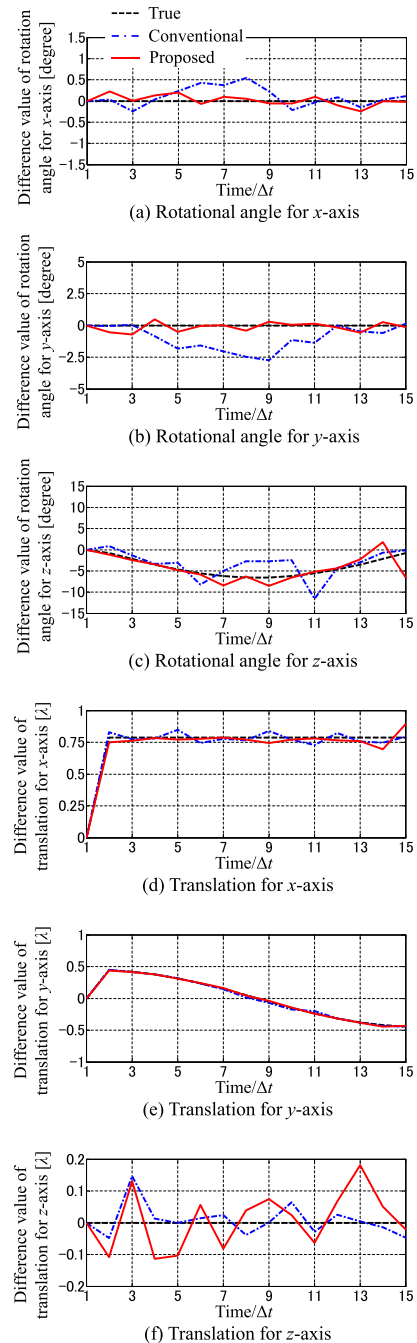
Fig. 17 Motion of target ♯1 for each observation time estimated by the conventional and proposed method in S/N = 25 dB. ((a) Difference value of rotation angle for x-axis (b) Difference value of rotation angle for y-axis (c) Difference value of rotation angle for z-axis (d) Difference value of translation motion for x-axis (e) Difference value of translation motion for y-axis (f) Difference value of translation motion for z-axis.)

compared to that obtained by the conventional method. Tables 1 and 2 summarize the comparison of the RMSE of the rotation angle, the translation motion, and the reconstructed image defined in Eq. (9) estimated using conventional and proposed methods at S/N = 25 dB for targets ♯1 and ♯2, respectively. These tables quantitatively verify that

(a) Rotational angle for *x*-axis

(b) Rotational angle for *y*-axis

(c) Rotational angle for *z*-axis

(d) Translation for *x*-axis

(e) Translation for *y*-axis

(f) Translation for *z*-axis

Fig. 18 Motion of target ♯2 for each observation time estimated by the conventional and proposed method in S/N = 25 dB. ((a) Difference value of rotation angle for *x*-axis (b) Difference value of rotation angle for *y*-axis (c) Difference value of rotation angle for *z*-axis (d) Difference value of translation motion for *x*-axis (e) Difference value of translation motion for *y*-axis (f) Difference value of translation motion for *z*-axis.)

each RMSE values for motion and shape estimation of the proposed method are significantly improved over those of the conventional method for each target.

7. Conclusion

This paper proposed a novel method of imaging and mo-
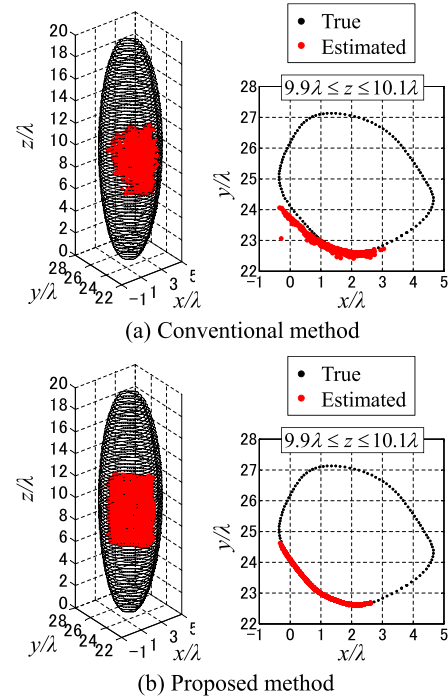
(a) Conventional method

(b) Proposed method

Fig. 19 Reconstructed image of target ♯1 in S/N = 25 dB. ((a) Conventional method (b) Proposed method.)

(a) Conventional method
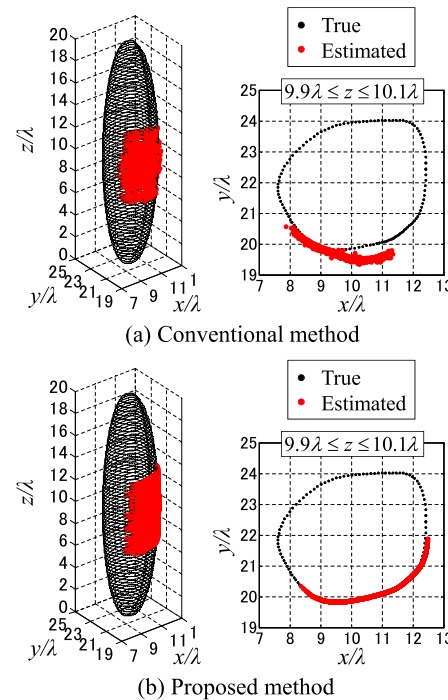
(b) Proposed method

Fig. 20 Reconstructed image of target ♯2 in S/N = 25 dB. ((a) Conventional method (b) Proposed method). (Upper: 3-dimensional view. Lower: cross section image for $9.9 \leq z \leq 10.1\lambda$.)

tion estimation for multiple moving targets, which is a substantial revision of the previous method [10]. The major novelty of this paper is that it exploits a unique feature of the RPM correct target clustering and one-to-one correspon-

Table 1 RMSE of the rotation angle, the translation motion and the reconstructed shape estimated by the conventional and proposed method for target ♯1 at S/N = 25 dB.

	Rotation angle	Translation	Reconstructed shape
Conventional	1.431°	0.034 λ	0.112 λ
Proposed	0.863°	0.047 λ	0.038 λ

Table 2 RMSE of the rotation angle, the translation motion and the reconstructed shape estimated by the conventional and proposed method for target ♯2 at S/N = 25 dB.

	Rotation angle	Translation	Reconstructed shape
Conventional	1.791°	0.035 λ	0.293 λ
Proposed	0.787°	0.032 λ	0.035 λ

dence between a target and range point, to suppress interference effects. In addition, this method adopts the Envelope method for estimating the normal vectors with greater accuracy. Combined with the target clustering achieved by the RPM method, the Envelope interpolation approach can enhance the motion estimation accuracy, especially for rotation angles, owing to the accurately estimated normal vectors. Results from numerical simulations for both 2-D and 3-D models indicate that the proposed method offers more robust and accurate estimation of both motion and shape of objects by reducing the range extraction error or by considering the amount the normal vector is displaced, and offers a significant advantage over the conventional method. However, there are some limitations concerning the target motion model or observational conditions as described in the final paragraph in Sect. 5. An important aspect of future work is to extend this method to more general and challenging models of practical use.

Acknowledgment

References

[1] D.L. Mensa, G. Heidbreder, and G. Wade, "Aperture synthesis by object rotation in coherent imaging," IEEE Trans. Nuclear Science, vol.27, no.2, pp.989–998, April 1980.

[2] A.J. Devaney, "Time reversal imaging of obscured targets from multistatic data," IEEE Trans. Antennas Propag., vol.53, no.5, pp.1600–1610, May 2005.

[3] E.A. Marengo, F.K. Gruber, and F. Simonetti, "Time-reversal MUSIC imaging of extended targets," IEEE Trans. Image Process., vol.16, no.8, pp.1967–1984, Aug. 2007.

[4] J. Song, Q.H. Liu, P. Torrione, and L. Collins, "Two-dimensional and three dimensional NUFFT migration method for landmine detection using ground-penetrating radar," IEEE Trans. Geosci. Remote Sens., vol.44, no.6, pp.1462–1469, June 2006.

[5] F. Soldovieri, A. Brancaccio, G. Prisco, G. Leone, and R. Pieri, "A Kirchhoff-based shape reconstruction algorithm for the multimonostatic configuration: The realistic case of buried pipes," IEEE Trans. Geosci. Remote Sens., vol.46, no.10, pp.3031–3038, Oct. 2008.

[6] S. Kidera, T. Sakamoto, and T. Sato, "Accurate UWB radar 3-D imaging algorithm for complex boundary without wavefront connection," IEEE Trans. Geosci. Remote Sens., vol.48, no.4, pp.1993–2004, April 2010.

[7] J.R. Fienup, "Detecting moving targets in SAR imagery by focusing," IEEE Trans. Aerosp. Electron. Syst., vol.37, no.3, pp.794–809, July 2001.

[8] A. Lin and H. Ling, "Doppler and direction-of-arrival (DDOA) radar for multiple-mover sensing," IEEE Trans. Aerosp. Electron. Syst., vol.43, no.4, pp.1496–1509, April 2007.

[9] T. Sakamoto and T. Sato, "Using a UWB radar imaging method with five antennas on a target with arbitrary translation and rotation motion," 5th European Conference on Antennas and Propagation (EuCAP), EUR Congressi, Rome, Italy, 11 April 2011.

[10] R. Yamaguchi, S. Kidera, and T. Kirimoto, "Accurate imaging method for moving target with arbitrary shape for multi-static UWB radar," IEICE Trans. Commun., vol.E96-B, no.7, pp.2014–2023, July 2013.

[11] S. Kidera, T. Sakamoto, and T. Sato, "A robust and fast imaging algorithm with an envelope of circles for UWB pulse radars," IEICE Trans. Commun., vol.E90-B, no.7, pp.1801–1809, July 2007.

[12] Federal Communications Commission (FCC), Office of Engineering and Technology (OET) Bulletin no.65, Supplement C, p.35, Aug. 1997.

[13] Y. Abe, S. Kidera, and T. Kirimoto, "Accurate image expansion method using range points based ellipse fitting for UWB imaging radar," IEICE Trans. Commun., vol.E95-B, no.7, pp.2424–2432, July 2012.

[14] S. Kidera, T. Sakamoto, and T. Sato, "A high-resolution imaging algorithm without derivatives based on waveform estimation for UWB pulse radars," IEICE Trans. Commun., vol.E90-B, no.6, pp.1487–1494, June 2007.

[15] J. Kennedy and R.C. Eberhart, "Particle swarm optimization," Proc. IEEE. Int. Conf. Neural Netw., pp.1942–1948, 1995.

[16] E. Miyagawa and T. Saito, "Particle swarm optimizers with growing tree topology," IEICE Trans. Fundamentals, vol.E92-A, no.9, pp.2275–2282, Sept. 2009.

Ryo Yamaguchi received his B.E. and M.E. degrees in Electronic Engineering from University of Electro-Communications in 2011 and 2013, respectively. He joined Hitachi, Ltd. Infrastructure Systems Company, in 2013.

Shouhei Kidera received his B.E. degree in Electrical and Electronic Engineering from Kyoto University in 2003 and M.I. and Ph.D. degrees in Informatics from Kyoto University in 2005 and 2007, respectively. He is currently an Associate Professor in Graduate School of Informatics and Engineering, the University of Electro-Communications, Japan. His current research interest is in advanced radar signal processing or electromagnetic inverse scattering issue for ultra wideband (UWB) sensor. He was awarded Ando Incentive Prize fo the Study of Electronics in 2012, Young Scientist's Prize in 2013 by the Japanese Minister of Education, Culture, Sports, Science and Technology (MEXT), and Funai Achievement Award in 2014. He is a member of the Institute of Electrical and Electronics Engineering (IEEE) and the Institute of Electrical Engineering of Japan (IEEJ).

Tetsuo Kirimoto received the B.S. and M.S. and Ph.D. degrees in Communication Engineering from Osaka University in 1976, 1978 and 1995, respectively. During 1978–2003 he stayed in Mitsubishi Electric Corp. to study radar signal processing. From 1982 to 1983, he stayed as a visiting scientist at the Remote Sensing Laboratory of the University of Kansas. From 2003 to 2007, he joined the University of Kitakyushu as a Professor. Since 2007, he has been with the University of Electro-Communications, where he is a Professor at the Graduate School of Informatics and Engineering. His current study interests include digital signal processing and its application to various sensor systems. Prof. Kirimoto is a senior member of IEEE and a member of SICE (The Society of Instrument and Control Engineers) of Japan.